Monthly Notices
of the
ROYAL ASTRONOMICAL SOCIETY

MNRAS **437,** 1962–1975 (2014)
Advance Access publication 2013 November 19

doi:10.1093/mnras/stt2027

Nova multiwavelength light curves: predicting UV precursor flashes and pre-maximum halts

Y. Hillman,[1]★ D. Prialnik,[1] A. Kovetz,[1,2] M. M. Shara[3] and J. D. Neill[4]

[1]*Department of Geophysics and Planetary Sciences, Raymond and Beverly Sackler Faculty of Exact Sciences, Tel-Aviv University, Tel-Aviv 69978, Israel*
[2]*School of Physics and Astronomy, Raymond and Beverly Sackler Faculty of Exact Sciences, Tel Aviv University, Tel-Aviv 69978, Israel*
[3]*Department of Astrophysics, American Museum of Natural History, Central Park West and 79th street, New York, NY 10024-5192, USA*
[4]*California Institute of Technology, 1200 E. California Blvd., Pasadena, CA 91125, USA*

Accepted 2013 October 18. Received 2013 October 17; in original form 2013 August 6

ABSTRACT

The dramatic brightenings of classical novae have yielded rich data sets of detailed light curves. Modelling these light curves is a challenge for any theory of classical novae. We have used our extended grid of nova outburst calculations to predict the luminosities of erupting novae expected in three electromagnetic bands – the visual, the near UV and the X-ray. Our models predict and explain many features of novae before eruption, as well as detailed characterizations of nova outbursts and post-nova declines. The evolutionary time-scales of eruption features vary by orders of magnitude, and depend on the basic nova parameters: white dwarf mass, luminosity and accretion rate. However, all light curves are found to share common features. Some of these features are unique to only one electromagnetic passband, while others show up in two, or in all three of the analysed bands. One extraordinary feature, common to all of our low-mass white dwarfs ($0.65\,M_{\odot}$) novae, is that all exhibit a sharp rise followed by a more gradual decline in the near-UV luminosity, prior to the eruption in the visual luminosity. This is because the expansion of the outer layers lags behind the rise in bolometric luminosity. These predicted precursor-UV-flashes last between a few hours and a few days, and the predicted luminosity increase is between ∼0.5 and ∼3 mag. These flashes should be easily observable if a nova event is detected early and its time coverage is dense. Many observed novae exhibit a pre-maximum halt, and this feature is found in all three electromagnetic bands of many, but not all, of our nova models. We explain the presence or absence of pre-maximum halts as due to changes in the convective energy transfer regime. Finally we note cases where the maximum visual magnitude reaches as high as −8.5 mag for low-mass white dwarfs. This re-emphasizes the fact that white dwarf mass is not always the determining factor in setting a nova's peak luminosity.

Key words: methods: data analysis – methods: numerical – binaries: close – novae, cataclysmic variables – white dwarfs.

1 INTRODUCTION

Classical novae (CNe) are powerful explosions of previously faint stars. The study of CN eruptions was energized by the appearance of first-magnitude GK Persei – Nova 1901 AD. Since then, many such energetic, mass-ejecting events have been detected, first in our own Galaxy (e.g. Payne-Gaposchkin 1957) and, more recently, in galaxies all the way out to the Virgo cluster. The physical explanation of the CN phenomenon followed Kraft's (1964) study, which demonstrated that novae must be composed of a white dwarf (WD) – the primary star – accreting hydrogen-rich matter via an accretion disc from a red dwarf (RD) companion – the secondary star. Two logical consequences of this model are that (1) CN are powered by thermonuclear runaways (TNR) in their WDs' hydrogen-rich envelopes (Starrfield et al. 1972) and (2) novae must self-extinguish when their erupting envelopes are ejected (Prialnik, Shara & Shaviv 1978).

Early theoretical studies focused on nova simulations of the accreting WD up to the TNR, using a hydrostatic stellar evolution code. The first full-cycle nova simulation was carried out by Prialnik (1986), on a main-frame computer, using a hydrodynamic code. The appearance of workstations, and of PCs with high speed and large memory, enabled carrying out simulations of several, consecutive cycles (Shara, Prialnik & Kovetz 1993; Prialnik & Kovetz 1995). It became clear (Prialnik 1995) that a simulation of a nova on a WD of given composition (e.g. C and O in equal mass fractions) depended on three key parameters: the WD mass $M_{\rm WD}$, its

★E-mail: yaelhill@post.tau.ac.il

(isothermal) core temperature T_c, and the accretion rate $\dot{M}$. Grids of nova simulations for wide ranges of these three parameters were calculated (Prialnik & Kovetz 1995), culminating with a determination of the *limits* of these ranges, outside of which novae could not occur (Yaron et al. 2005).

A typical nova cycle comprises an accretion phase, an eruption followed by a mass-loss phase and a long decline that overlaps the next accretion phase (Prialnik 1986). A nova eruption starts when a TNR is initiated in an accreting WD's envelope (Shara 1989; Starrfield, Iliadis & Hix 2008). A rise in visual luminosity has signalled the vast majority of novae outbursts to astronomers, but we note that, until the past two decades, most novae were not intensively observed in the ultraviolet or X-ray passbands. During the late stages of nova eruptions, after mass loss has ceased, the visual (VIS) luminosity declines to its pre-nova value, while the near-UV (NUV) luminosity dominates (MacDonald, Fujimoto & Truran 1985). Eventually, it declines as well. The X-ray luminosity also remains high after the decline in the VIS luminosity Itoh & Hachisu (1990); MacDonald & Vennes (1991). It has been observed in novae decades after the visual eruption has ended. Finally, it declines as well (Orio et al. 1994, 2009; Schaefer & Collazzi 2010).

Simulations of nova outburst evolution show that the rise in bolometric luminosity L following the onset of the TNR occurs at almost constant radius. This is because the dynamical expansion time of the WD envelope – hours to days – is much longer than the time-scale of the last explosive phase of the TNR – minutes. The net result is that the effective temperature $T_{\rm eff}$ of a nova rises very rapidly, at the TNR time-scale. When L approaches the Eddington limit, the WD's outer layers start expanding at almost constant (Eddington) luminosity, and the effective temperature decreases as the radius increases and the mass loss phase begins. We expect this general behaviour to be reflected in the evolution of the luminosities in the VIS, NUV and X-ray passbands; but we are aware of significant variations in outburst behaviours amongst our many models. These variations, in addition to recent detailed observations and classification schemes of nova light curves (Strope, Schaefer & Henden 2010), have motivated us to data-mine the extensive data base generated by the calculations of Prialnik & Kovetz (1995) and Yaron et al. (2005) (see Section 3) in order to confront nova model light curves with observations.

In the next section we describe the general physical principles that govern the behaviour of nova luminosities in different passbands. In Section 3 we describe the data base used for this study. In Section 4 we analyse the results of our study. A brief discussion and main conclusions follow in Section 5.

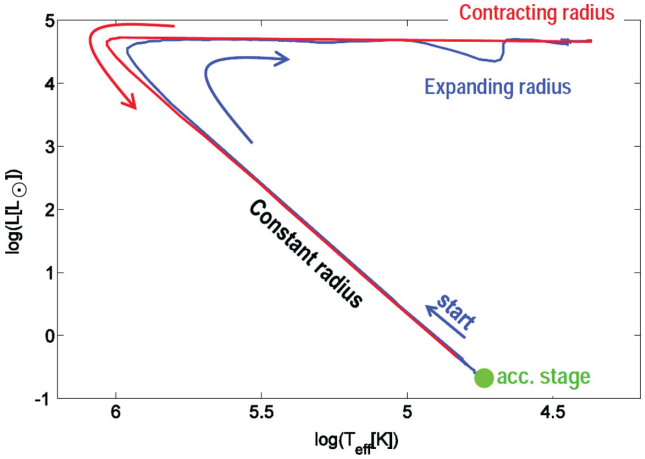

Figure 1. A full, typical nova cycle shown in an HR diagram, for the parameter combination; $M_{\rm WD} = 1.25\,{\rm M}_\odot$, $T_{\rm c} = 5 \times 10^7$ K and $\dot{M}_{\rm WD} = 10^{-10}\,{\rm M}_\odot\,{\rm yr}^{-1}$.

2 THE EVOLUTION OF NOVA LUMINOSITY, TEMPERATURE AND RADIUS

Fig. 1 shows the path of the luminosity and the effective temperature of a typical nova cycle in an HR diagram. A significant part of the nova cycle is spent during the accretion phase, in quiescence, i.e. both $T_{\rm eff}$ and L remain constant. The onset of the nova eruption is marked by the rapid rise of $T_{\rm eff}$ and L along a slope of constant radius. This is followed by the expansion and the mass-loss stage, represented by the turn to the right, and a subsequent horizontal path. As mass-loss declines, contraction of the envelope ensues, illustrated by the turn back towards higher effective temperatures along the same horizontal line. Finally, when mass ejection stops, L and $T_{\rm eff}$ revert slowly back to their pre-nova values, descending along the same slope, at constant radius, as the rapid rise to maximum light.

The typical evolution in time of a nova flash (effective temperature, radius and luminosity) emerging from Fig. 1 is displayed in Fig. 2 for a $1.25\,{\rm M}_\odot$ WD, a core temperature of 5×10^7 K and an accretion rate of $10^{-10}\,{\rm M}_\odot{\rm yr}^{-1}$. The left panel shows a complete

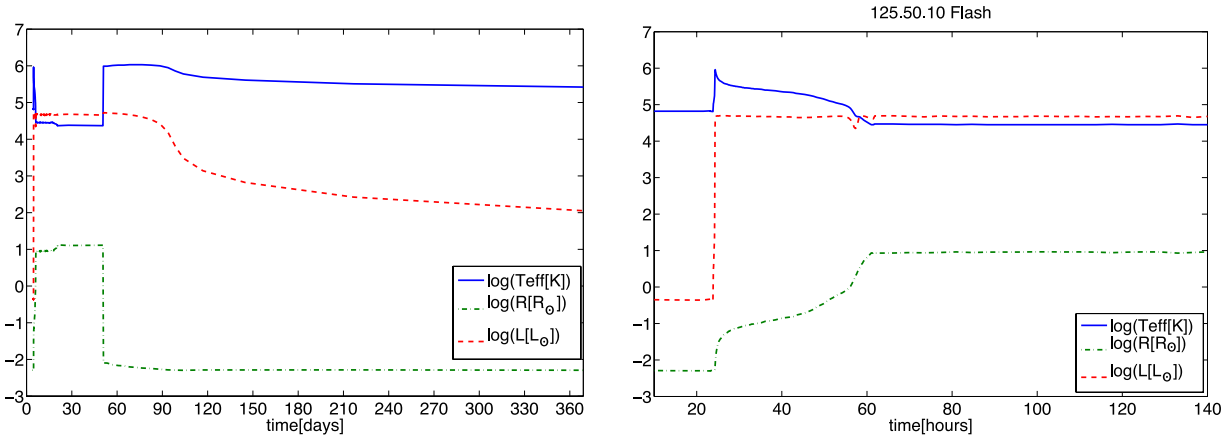

Figure 2. Evolution of $\log(T_{\rm eff}[{\rm K}])$ (blue solid), $\log(R[{\rm R}_\odot])$ (green dash–dotted) and $\log(L[{\rm L}_\odot])$ (red dash) for $M_{\rm WD} = 1.25\,{\rm M}_\odot$, $T_{\rm c} = 5 \times 10^7$ K and $\dot{M}_{\rm WD} = 10^{-10}\,{\rm M}_\odot\,{\rm yr}^{-1}$. Left: a complete light curve on a time-scale of days. Right: a close-up of the pre-nova temperature spike (time-scale of hours).

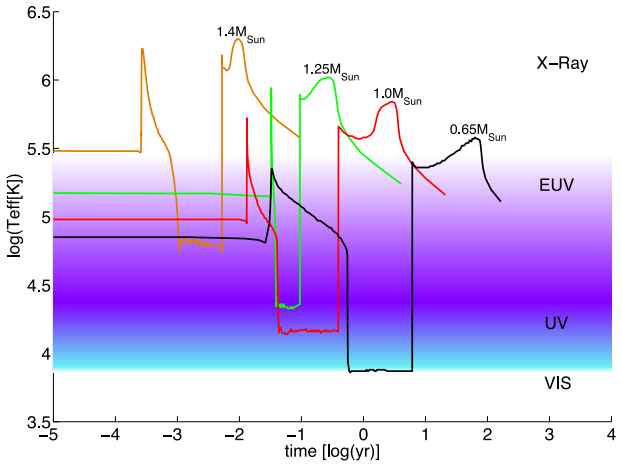

Figure 3. Evolution of $\log(T_{\rm eff}[{\rm K}])$ throughout a nova cycle for a WD central temperature of $T_{\rm c} = 10^7$ K, an accretion rate of $\dot{M}_{\rm WD} = 10^{-8}\,{\rm M}_{\odot}\,{\rm yr}^{-1}$ and the masses: $M_{\rm WD} = 0.65\,{\rm M}_{\odot}$ (black); $M_{\rm WD} = 1.0\,{\rm M}_{\odot}$ (red); $M_{\rm WD} = 1.25\,{\rm M}_{\odot}$ (green); and $M_{\rm WD} = 1.4\,{\rm M}_{\odot}$ (orange).

nova outburst. Note the initial sharp spike in the effective temperature during the first day, which then declines as the radius expands. The right panel of Fig. 2 shows a close-up of this temperature spike.

The effective temperatures displayed by all novae undergo drastic changes throughout a nova outburst, regardless of the three key nova parameters. Fig. 3 shows the behaviour of $T_{\rm eff}$ throughout a complete nova cycle on a logarithmic scale, as well as the common features and differences in the $T_{\rm eff}$ profile for different WD masses. The cycle duration and the minimum and maximum $T_{\rm eff}$ vary depending on the chosen key parameter values (e.g. the WD mass). However, in all cases, $T_{\rm eff}$ changes by ∼1–2 orders of magnitude throughout the cycle, causing the wavelength of peak emission to pass through the various electromagnetic bands. This results in the apparent magnitude evolving in very different manners for the different electromagnetic bands. This behaviour is described in more detail in Section 4.

The accretion rate indirectly affects the light curves as well: a faster accretion rate results in a shorter time-scale for mass ejection. But the most important information gleaned from these light curves is that the duration of the effective temperature peak ranges from a few hours to a few months, a testable prediction for each of the VIS, NUV and XRT passbands.

3 DATA BASE

The data base for this study is the grid of nova light curves derived from modelling by Prialnik & Kovetz (1995) and then expanded by Yaron et al. (2005). The grid spans a range of values for the three parameters; the WD mass ($M_{\rm WD}$: 0.65, 1.0, 1.25 and $1.4\,{\rm M}_{\odot}$), the core temperature ($T_{\rm c}$: 10^7, 3×10^7 and 5×10^7 K) and the accretion rate ($\dot{M}_{\rm WD}$: 10^{-7}, 10^{-8}, 10^{-9}, 10^{-10}, 10^{-11} and $10^{-12}\,{\rm M}_{\odot}\,{\rm yr}^{-1}$). The nova evolution code used to derive the light curves is a hydrodynamic Lagrangian code and was described in some detail by Prialnik & Kovetz (1995). It includes OPAL opacities, a nuclear reaction network including 40 heavy element isotopes up to ^{31}P, convection according to the mixing-length theory, diffusion for all elements, accretional heating and a mass-loss algorithm that applies a steady, optically thick supersonic wind solution. The dynamical phases are calculated by solving the equation of motion along with the energy balance equation, rather than imposing hydrostatic equilibrium. Mass loss is calculated continually, according to the mass-loss rate $\dot{M}_{m-l}$ derived from the optically thick wind solution.

For each parameter combination, the code was programmed to run for ∼5–10 consecutive cycles, until a regular cyclic pattern was obtained, showing very little variations between the cycles (of the order of a few per cent). Then one cycle was selected for extensive analysis. The nova parameters in the following figures are specified in the figure title in the form: '$M_{\rm WD}.T_{\rm c}.\dot{M}_{\rm WD}$', e.g. 125.30.9 refers to the model; $M_{\rm WD} = 1.25\,{\rm M}_{\odot}$, $T_{\rm c} = 3\times10^7$ K and $\dot{M}_{\rm WD} = 10^{-9}\,{\rm M}_{\odot}\,{\rm yr}^{-1}$. Data – in particular, the WD radius ($R_{\rm WD}$), $T_{\rm eff}$, L and visual magnitude ($M_{\rm V}$) – were produced for a large number of parameter combinations throughout the nova cycle. We then extracted the NUV and X-ray magnitudes ($M_{\rm NUV}$ and $M_{\rm XRT}$). The synthetic magnitudes are based on the response functions of the Galaxy Evolution Explorer (*GALEX*) Martin et al. (2005) NUV band, the SWIFT Gehrels et al. (2004) X-ray Telescope[1] (XRT), and the Johnson *V*-band filter Bessel (1990). The *GALEX* project has recently been terminated; we used the *GALEX* passband simply because we had easy access to it. However, the NUV wavelength span observed by *GALEX* is 175–280 nm Martin et al. (2005), while that observed by SWIFT UVOT is the nearly identical 170–290 nm.[2] Since the NUV passbands of the two telescopes cover almost the same wavelengths, the NUV light curves we produced for the *GALEX* passband are equally applicable to SWIFT UVOT observations. The model effective temperature and radius at a given point were used to specify the spectral energy distribution and luminosity of a blackbody. The response curves were used to integrate the blackbody flux within each of the passbands. The integrated fluxes were then converted to standard AB magnitudes Oke (1974). To simulate observations of the modelled novae in the nearby galaxy M31, we dim these magnitudes by a distance modulus of 24.4 mag Ribas et al. (2005).

4 ANALYSIS OF RESULTS

The 54 light curves analysed in this study are presented in the seven panels of Fig. 4. These show the evolution of nova luminosities in the VIS, NUV and XRT passbands. The $t = 0$ point is determined arbitrarily for the sake of plotting the light curves in a more or less similar fashion. The evolution time is measured continuously from the beginning of the first cycle for each evolution run. We systematically vary the three key WD parameters between successive models. Dramatic changes often occur when we vary just one parameter; changes in two parameters sometimes affect results in opposing directions, while changes in all three parameters lead to unpredictable results.

There are a few features that are common to all our light curves. X-ray emission is always minimal during the mass-loss phase, when the hot WD is obscured by its X-ray absorbing envelope. X-ray emission is highest during the post-nova decline, when mass loss has ceased and the hot WD is exposed. During the post-nova decline the VIS is always the lowest of the three luminosities as the hot WD emits mostly NUV and X-rays.

The time-scale of nova eruptions varies from about one day to tens of years, depending mostly on the WD mass. The accretion rate plays a secondary but non-negligible role. The *ratio* between the durations of the three nova phases – pre-nova rise, mass-loss phase

[1] http://swift.gsfc.nasa.gov/docs/heasarc/caldb/data/swift/xrt/index.html
[2] http://swift.gsfc.nasa.gov/analysis/uvot_ugrism.html

and post-nova decline – is roughly the same for all the models. The pre-nova rise time is always much shorter than the mass-loss time-scale which, in turn, is always much shorter than the post-nova decline time. The first of these is controlled by the dynamical time-scale of the WD envelope. The second is the time-scale required to generate sufficient nuclear energy to unbind the WD envelope. The third is the thermal time-scale of the outer WD and the remnant envelope not ejected by the nova.

4.1 Pre-Nova NUV flashes

The most important finding (and prediction) of this paper (based on the models published in 2005 by Yaron et al.) is that a subset of our models displays a bright flash in the NUV prior to the onset of the mass-loss phase. This NUV precursor (to the optical outburst) flash is exhibited by the low-mass, 0.65 $M_{\odot}$, WDs (all but the cold, extremely slow accreting 065.10.11) and occurs concurrently with the $T_{\rm eff}$ early peak. The amplitude of the NUV flashes varies from 0.5 to 2 mag and the duration is ∼5–10 d. There is one model, the 065.10.10 (Fig. 4, panel 1), that produces an exceptionally large flash – a magnitude change of ∼3 mag, which lasts as long as 60 d.

At least two observational detections of this phenomenon have recently been reported, based on *GALEX* observations of M31 novae. In particular, Cao et al. (2012) report that *'Novae M31N 2009-10b and M31N 2010-11a show prominent UV emission peaking a*

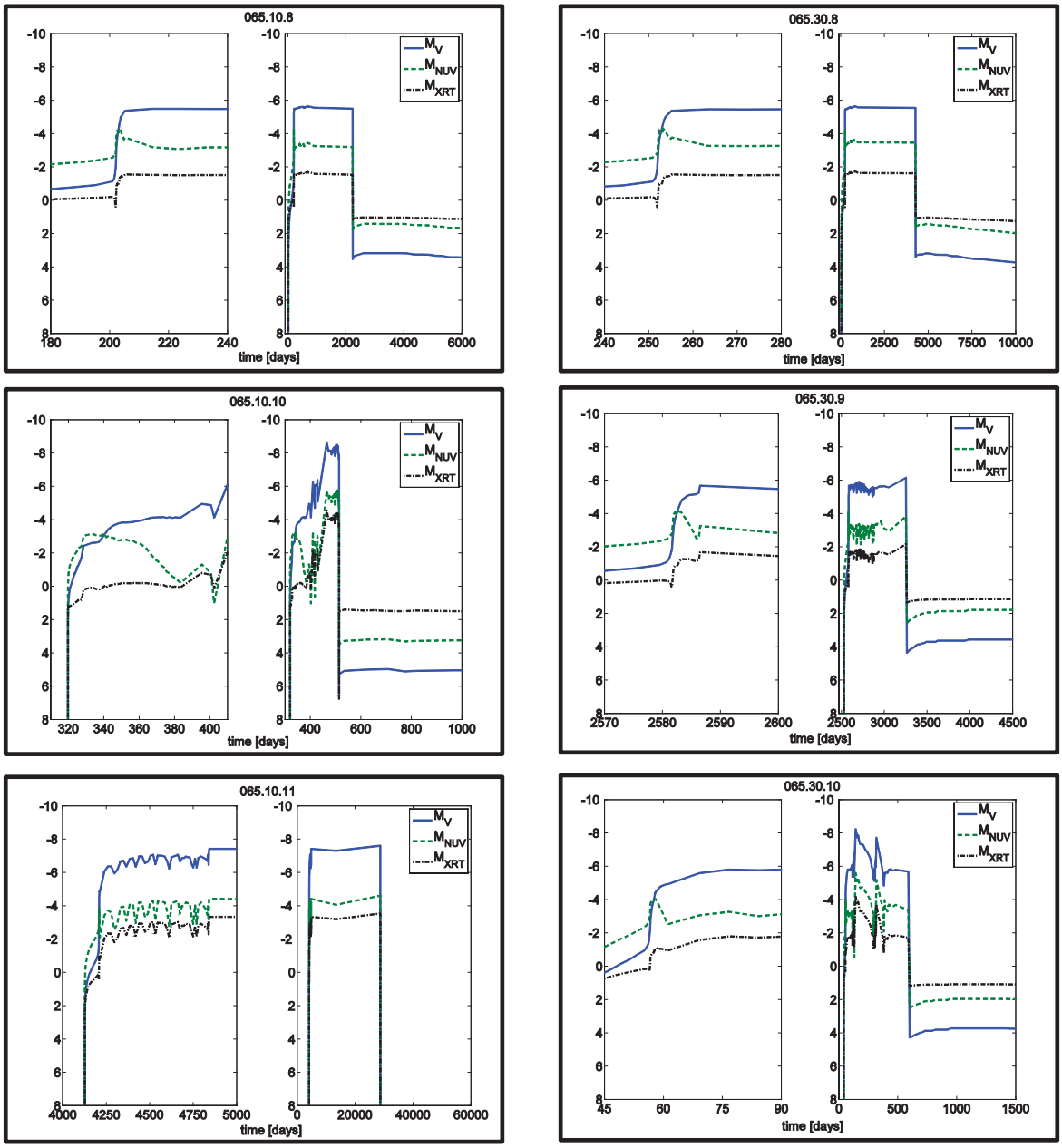

Figure 4. Panel 1. Light curves of a typical nova cycle for each parameter combination, given in $M_{\rm V}$ (solid blue), $M_{\rm NUV}$ (green dash) and $M_{\rm XRT}$ (black dash–dotted). Each light curve is given in its entirety in the right panel, while the left panel is a close up of its pre-nova rise. While the ordinate, representing the magnitude, is uniformly set for all the light curves, the abscissa, representing the time in days, changes depending on the time-scale of the specific nova model. The zero-point is arbitrary to some extent.

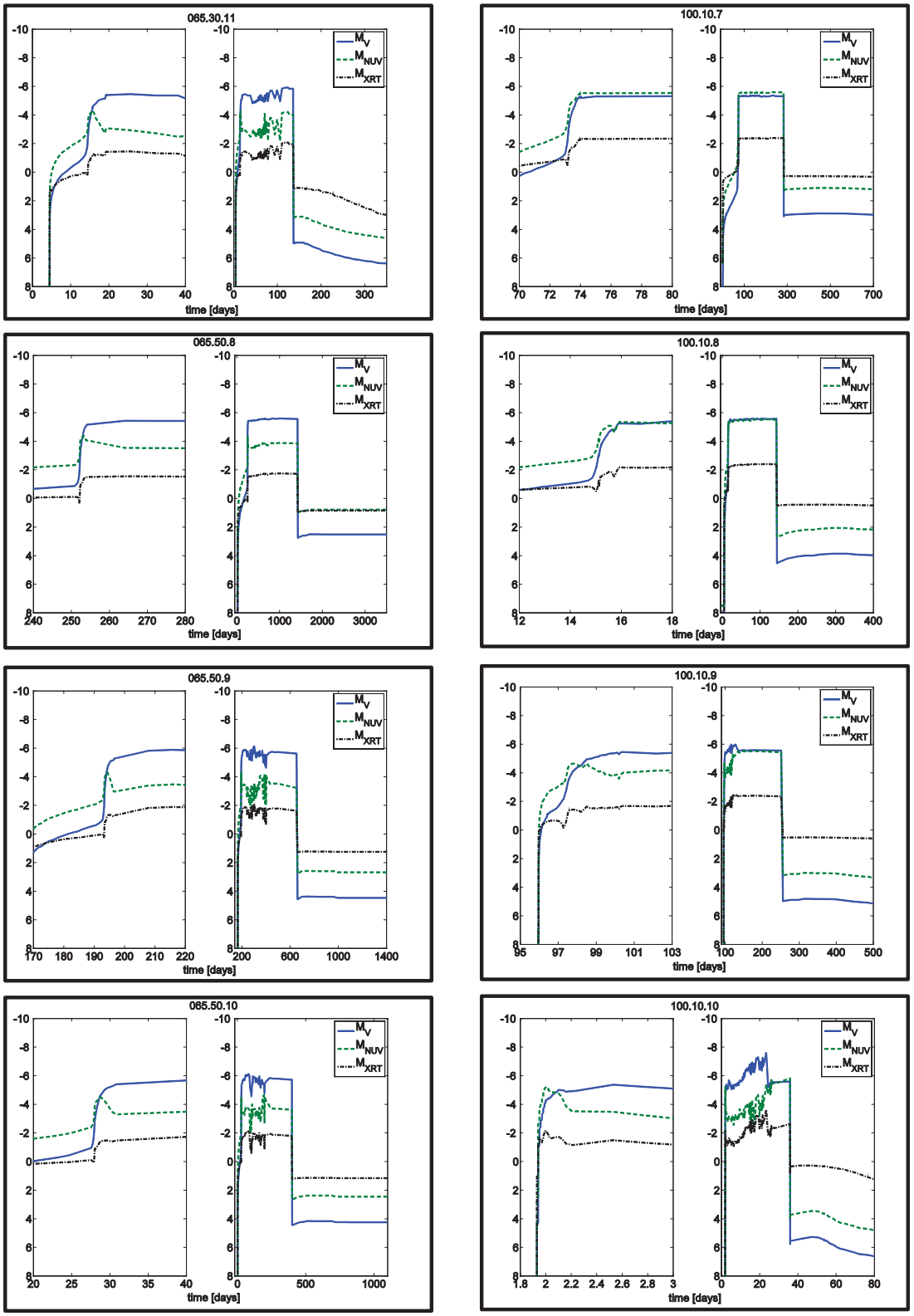

Figure 4. Panel 2.

few days prior to their optical maxima, possibly implying aspherical outbursts'. In Fig. 5 we reproduce the *R*-band and NUV light curves [from fig. 12 of Cao et al. (2012)], and superpose the VIS and NUV curves from our nova model 065.30.11 (Fig. 4, panel 2). The match is remarkably good.

Pietsch et al. (2007a) reported two cases where the UV emission was detected previous to the optical maximum: M31N 2007-07c and M31N 2007-07d. For M31N 2007-7c the Swift UV detection preceded the optical by 2.8 h Pietsch et al. (2007b), resembling our model 065.30.11 as well (Fig. 4, panel 2 and Fig. 5).

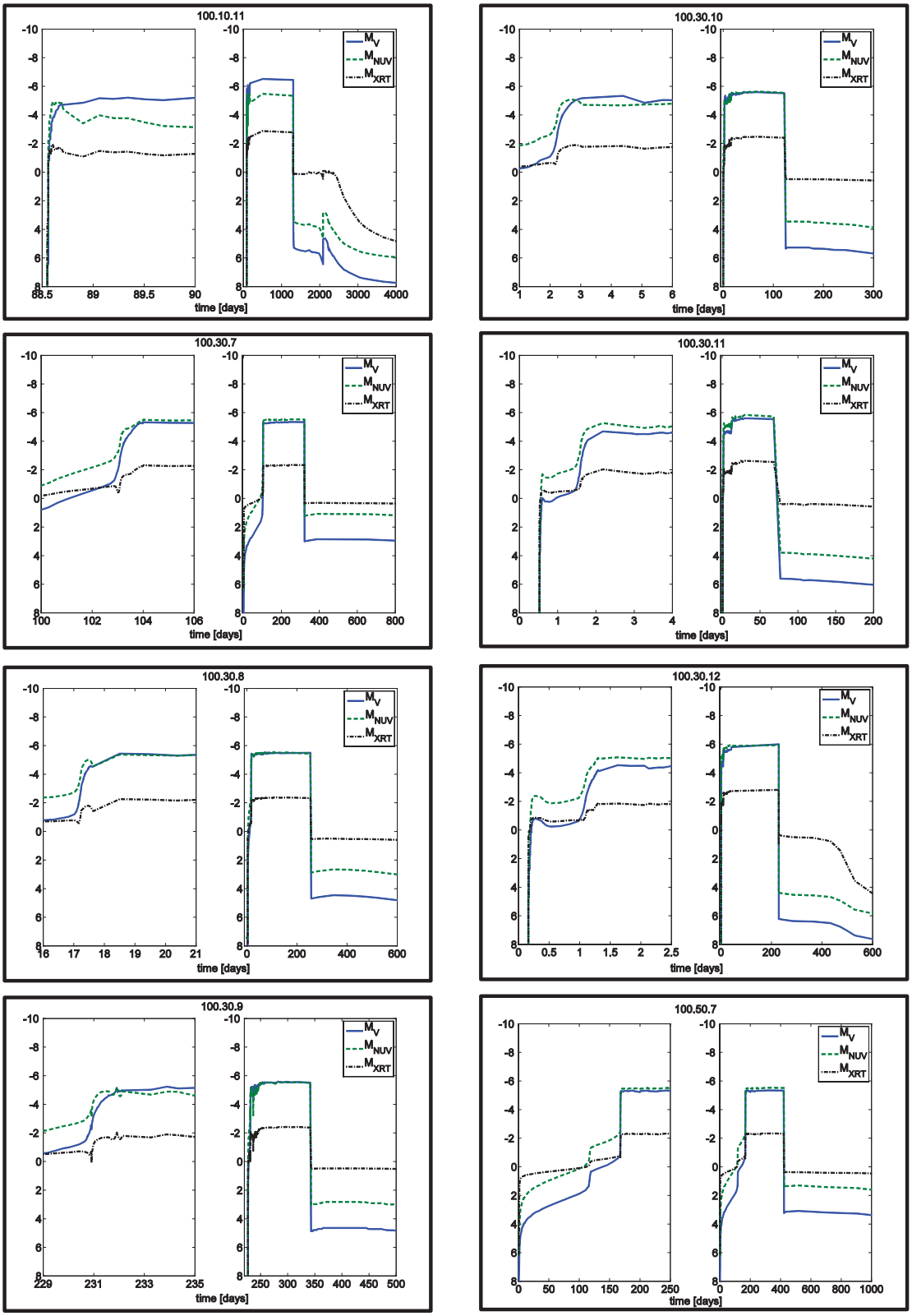

Figure 4. Panel 3.

Cao et al. (2012) also noted that *'the UV observations and the colour information suggest that UV and optical emission originate from different radiative regions because they cannot be simply interpreted as the thermal radiation of a receding spherical photosphere which has a large optical depth in local thermal equilibrium. Because UV emission is only generated deep inside the envelope, the result may suggest that the envelope has holes from which we can see deep inside.'* Our 065.30.11 model [see in particular table 2 of

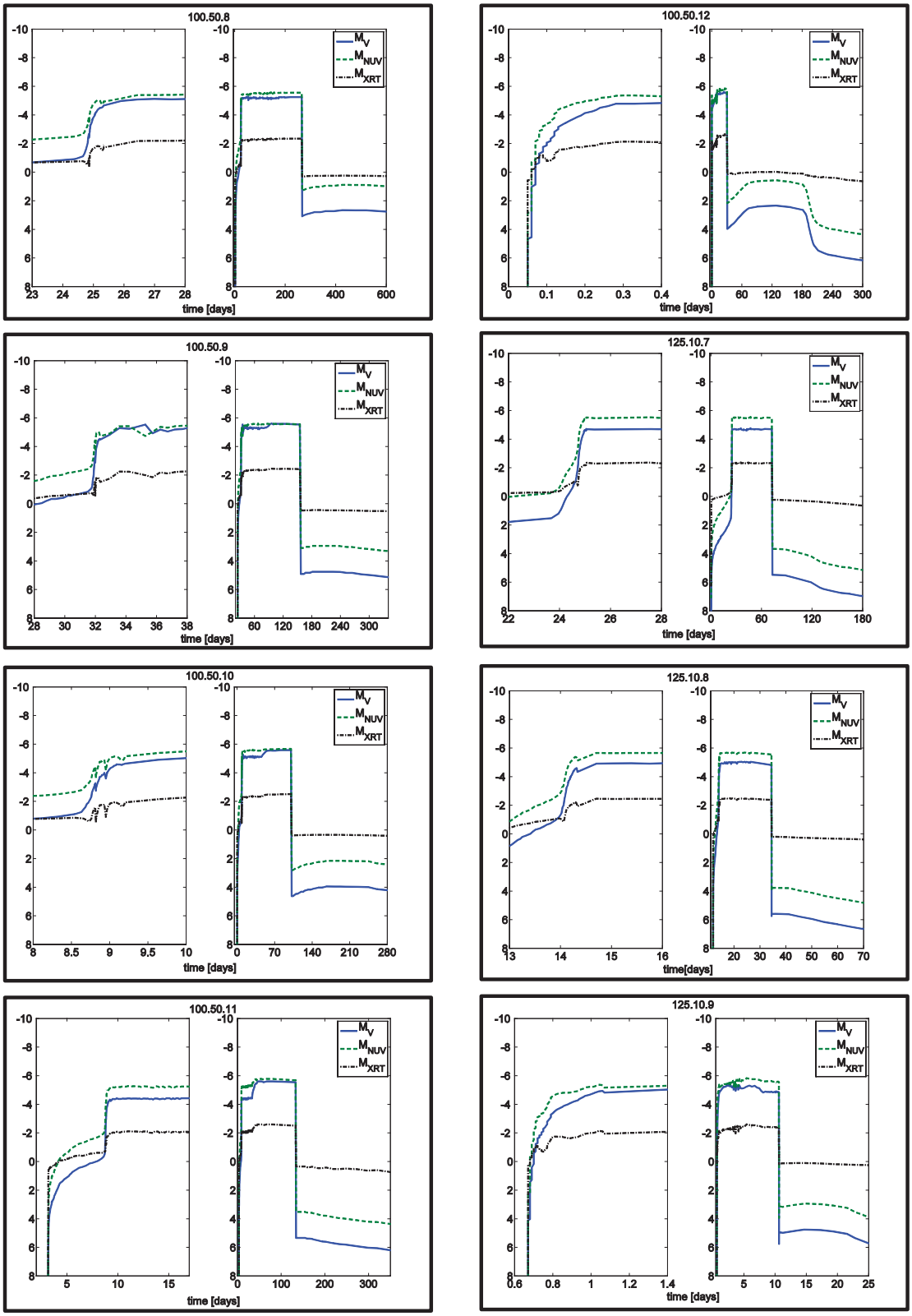

Figure 4. Panel 4.

Yaron et al. (2005)] suggests a much simpler explanation, consistent with the NUV maximum luminosity seen 2−3 d *before* optical maximum. The low-mass, slowly accreting WD must accumulate a hydrogen-rich envelope of $6 \times 10^{-5}\,M_{\odot}$ before a TNR can begin. During the 6×10^{6} years of accretion, diffusion mixes hydrogen into the CO WD outer envelope and CO into the hydrogen-rich envelope. The net result is that $9.5 \times 10^{-5}\,M_{\odot}$ – a massive nova envelope – must be heated sufficiently to escape the gravitational

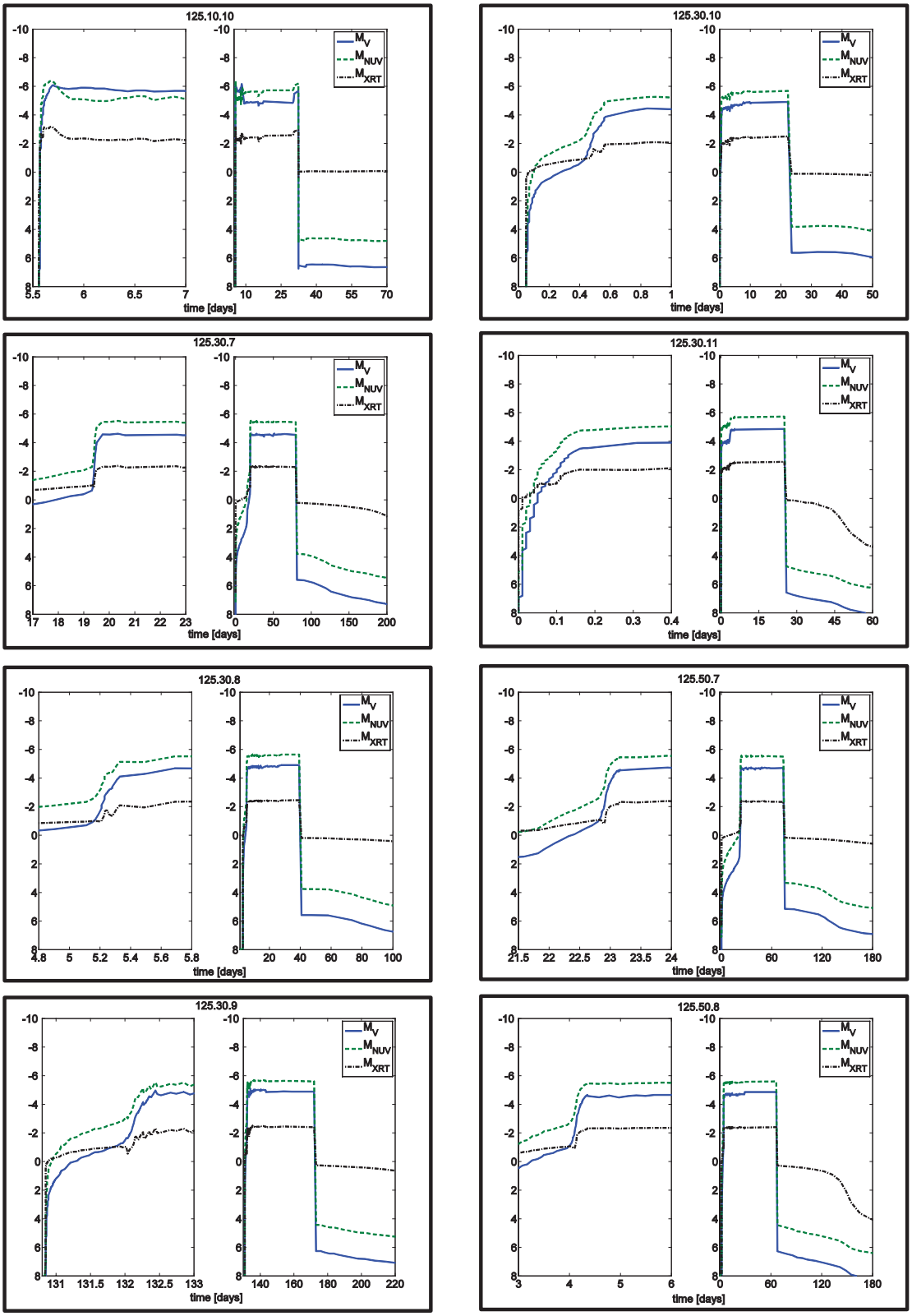

Figure 4. Panel 5.

grip of its WD. The low mass and large radius of the WD result in a relatively low pressure and weak TNR which reaches a maximum temperature of only 1.2×10^8 K. Thus, several days (rather than just a few hours, as for most novae) are required to release enough nuclear energy to significantly expand the massive envelope away from the WD.

During the several days that the envelope is hot but WD-sized it radiates mostly in the NUV. Thus we propose that nova

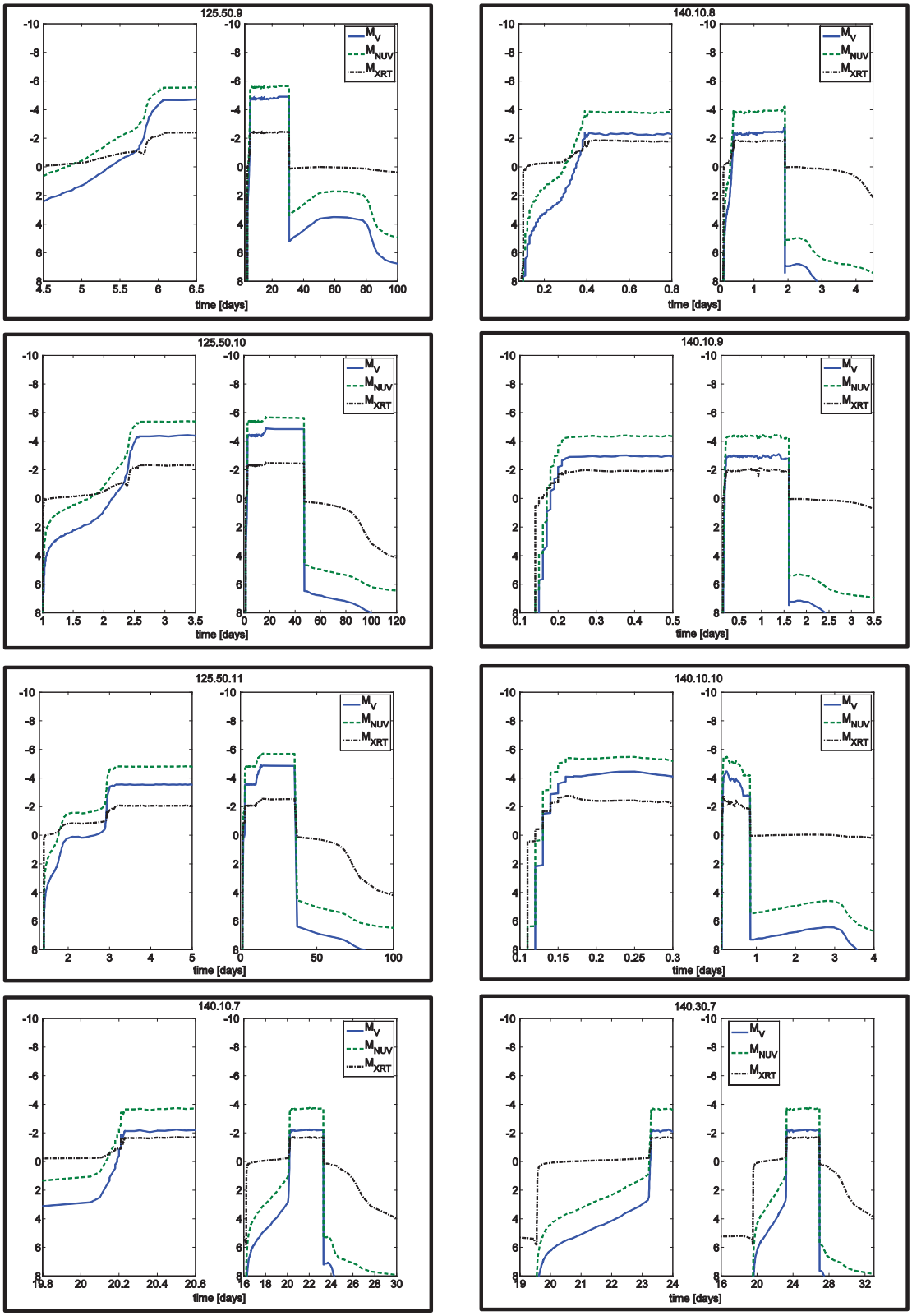

Figure 4. Panel 6.

NUV precursors, or flashes, like those seen in M31N 2009−10b and M31N 2010−11a are the result of a very slow WD envelope expansion, and not because of any inhomogeneity in the ejecta.

4.2 Symbiotic novae emission line flashes – a prediction

Exactly the same behaviour should occur for TNRs on WDs accreting from red giant (RG) companions – the symbiotic novae. The

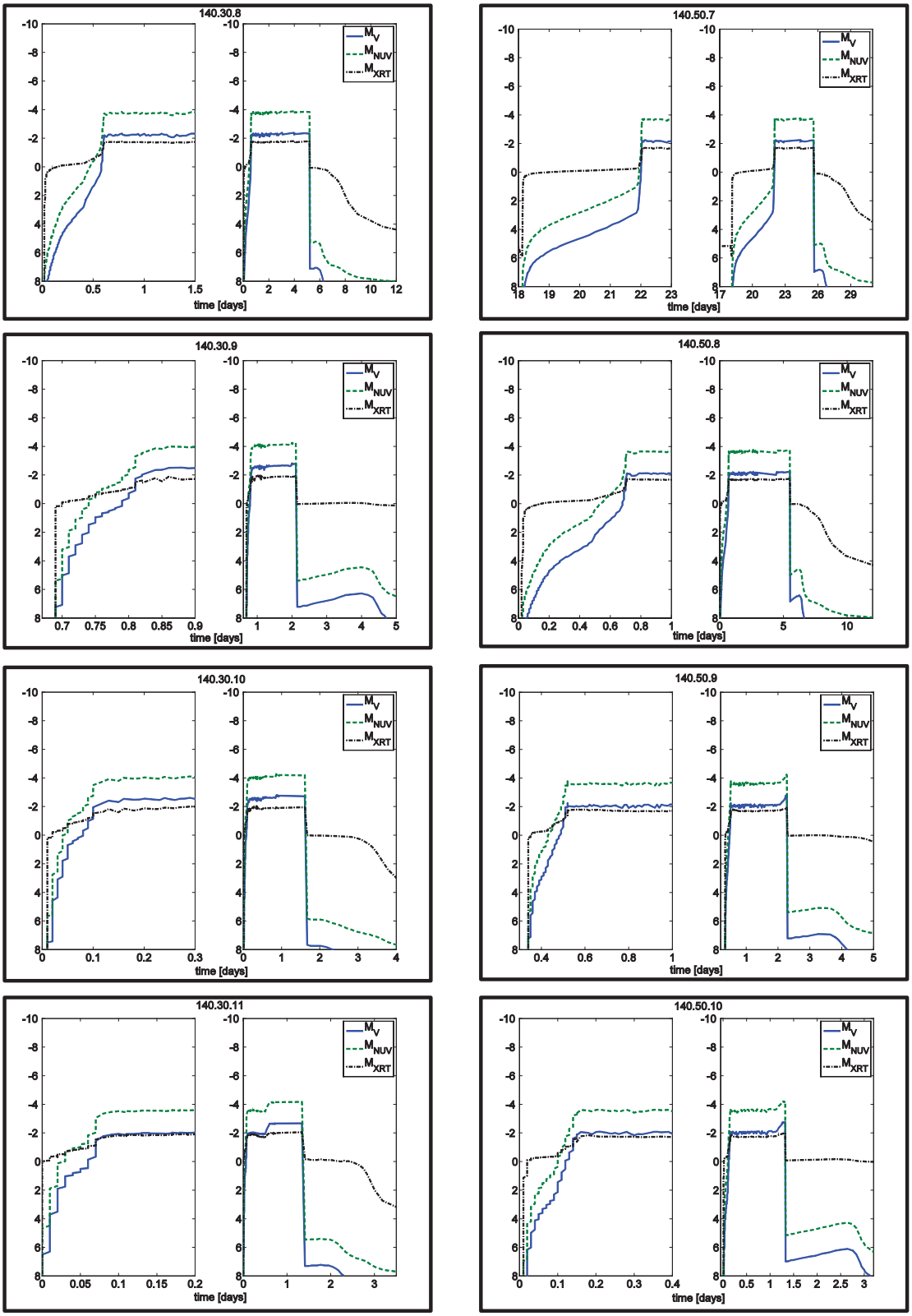

Figure 4. Panel 7.

WD NUV flashes on low-mass WDs that precede the optical flashes should irradiate their RG companions with high ionization potential photons. This should lead to a very rapid (minutes to a few hours) change in the emission-line spectra of the irradiated RGs. High excitation lines of helium, oxygen, iron and other elements should 'turn on' very quickly in the atmosphere of the RG, in response to the hard radiation suddenly being emitted by the erupting WD. This effect may have already been seen in the narrow UV emission

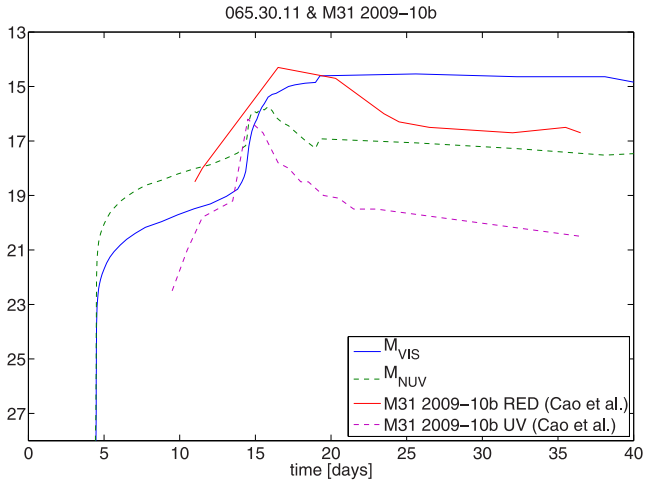

Figure 5. $M_{\rm WD} = 0.65\,{\rm M}_{\odot}$, $T_{\rm c} = 3 \times 10^7$ K and $\dot{M}_{\rm WD} = 10^{-11}\,{\rm M}_{\odot}\,{\rm yr}^{-1}$ superposed over the *R*-band and NUV of nova M31N 2009−10b from fig.12 in Cao et al. (2012). The magnitude scale of the model curves has been shifted to allow for comparison.

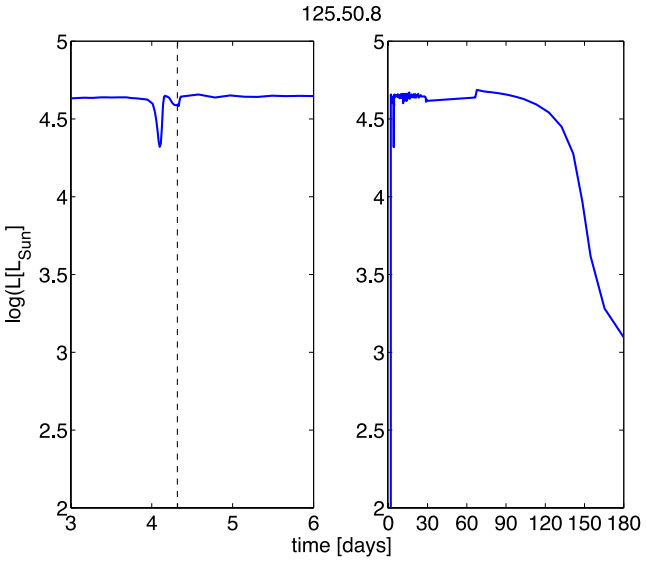

Figure 6. A luminosity dip accompanying a typical pre-maximum halt, shortly after reaching plateau and prior to mass loss for: $M_{\rm WD} = 1.25\,{\rm M}_{\odot}$, $T_{\rm c} = 5 \times 10^7$ K and $\dot{M}_{\rm WD} = 10^{-8}\,{\rm M}_{\odot}\,{\rm yr}^{-1}$ (see model 125.50.8 in Fig. 4, panel 5). The vertical dotted line marks the beginning of the mass-loss episode.

line component of RS Oph, shortly after its 1985 eruption Shore, Kenyon & Sonneborn (1996) and in the X-ray emission of RS Oph during its 2006 outburst. The problem may, however, be that even at those relatively early times, ejecta were already interacting with the pre-outburst wind Bode et al. (2006), thus complicating any such searches.

4.3 Pre-Nova X-ray flashes

A few intermediate-mass, cold, slow-accreting WD models, namely 100.10.10 (Fig. 4, panel 2), 100.10.11 (Fig. 4, panel 3) and 125.10.10 (Fig. 4, panel 5) exhibit a precursor X-ray flash in addition to the NUV flash. Because these WDs have smaller radii than those of the $0.65\,{\rm M}_{\odot}$ models, they produce significantly higher values of $T_{\rm eff}$ for the same luminosity, leading to an X-ray flash. The amplitude of the X-ray flashes is smaller than that of the NUV flashes: ∼0.5–1 mag. The duration of both the NUV and X-ray flashes on these more massive WDs is much shorter than for the $0.65\,{\rm M}_{\odot}$ models, a matter of 6–12 h.

Most of the $1.0\,{\rm M}_{\odot}$ models also brighten greatly in the NUV. Even during the expansion phase the effective temperature remains too high to allow the NUV luminosity to drop, and so the NUV and VIS luminosities remain comparable during the nova eruption. These WDs also undergo pre-maximum NUV halts, as we now explain.

4.4 Pre-maximum halts

For many of our models we find pre-maximum halts in the different electromagnetic bands; some show the halt in all three bands and others in only one or two. The halts come in different shapes and sizes, ranging from a fraction of a magnitude up to ∼5–6 mag, and a few even display a double halt. A common behaviour of the luminosities emitted in all three passbands is to increase as $T_{\rm eff}$ rises, and then to halt as $T_{\rm eff}$ declines. When mass loss begins, the luminosity rises to its maximum value.

An interesting feature accompanying the pre-maximum halt in many cases is a dip in the total luminosity (see Fig. 6). This dip occurs in conjunction with the decline of $T_{\rm eff}$ from its peak, just before mass loss begins. The cause of this dip is a temporary drop in the energy flux as convection in the expanding, thinning envelope ceases to be efficient near the envelope surface. The accompanying decrease in opacity soon allows radiation to take over from convection, halting and reversing the dip.

Some models produce a double halt, while the second halt is usually shorter, with a smaller amplitude and does not always show up in all three bands. Model 100.10.8 (Fig. 4, panel 2) exhibits a second halt with an amplitude of about a tenth of a magnitude in the visual luminosity and lasts a few hours, while in the NUV and X-ray luminosities the amplitude is five times larger (∼0.5 mag) and lasts twice as long. This particular second small halt (a close up is presented in Fig. 7) bears a remarkable resemblance to visual

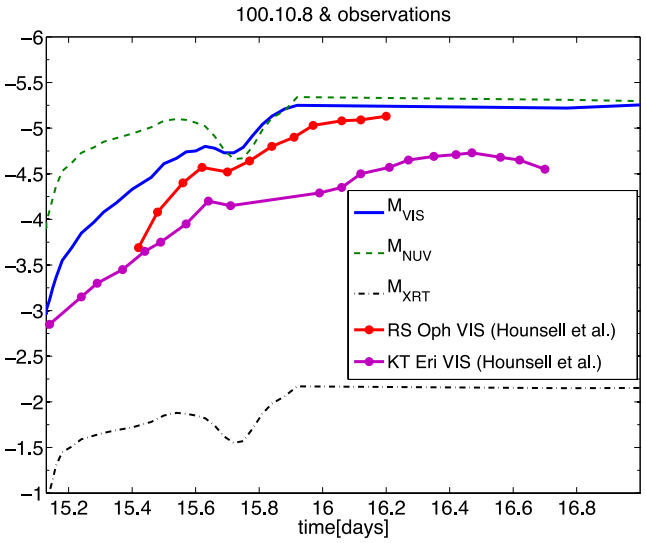

Figure 7. Close up of a pre-maximum halt resembling observations; $M_{\rm WD} = 1.0\,{\rm M}_{\odot}$, $T_{\rm c} = 10^7$ K and $\dot{M}_{\rm WD} = 10^{-8}\,{\rm M}_{\odot}\,{\rm yr}^{-1}$ superposed over the visual observations of RS Oph and KT Eri from Hounsell et al. (2010). The magnitude scale of the curves has been shifted to allow for comparison.

observational data of RS Ophiuchi and KT Eridani from Hounsell et al. (2010). The massive 125.10.8 model (Fig. 4, panel 4) shows a somewhat similar halt as well.

4.5 Oscillations

Prior to, or during the mass-loss phase, some of our models displayed luminosity oscillations of ∼0.5–1 mag in all three passbands. Time-scales ranged from ∼2 h to ∼50 d. These oscillations are caused by the restructuring and rebalancing that the envelope undergoes as it begins to expand. A typical example is model 125.30.9 (Fig. 4, panel 5), performing ∼ five small-amplitude oscillations (∼0.5 mag) over a period of ∼days. An exceptional case is model 065.10.11 (Fig. 4, panel 1) with ∼10 oscillations and an amplitude of ∼1 mag continuing for ∼500 d. Strope et al. (2010) have classified a data base of 93 well-observed nova light curves into seven morphological types, *oscillations* being one of them, based on the first 500 d after nova eruption. The light curve of model 065.30.9 (Fig. 4, panel 1) begins oscillating after reaching peak luminosity (Fig. 8) resembling the O-class (*oscillations*) nova light curves from Strope et al. (2010; see their fig. 13).

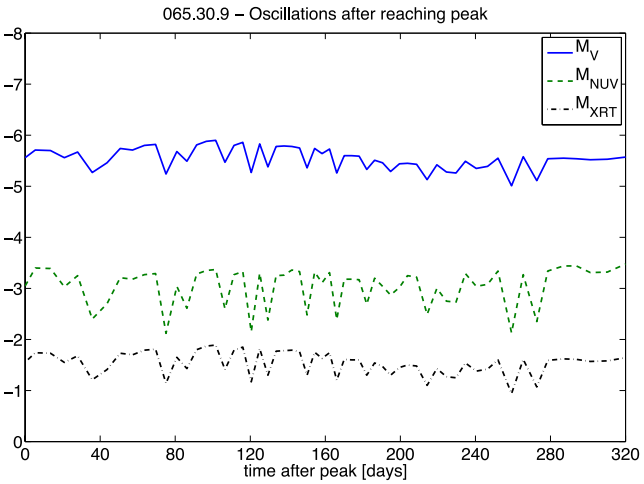

Figure 8. Close up of oscillations resembling Strope et al.'s (2010) O-class nova light curves; $M_{\rm WD} = 0.65\,{\rm M}_{\odot}$, $T_{\rm c} = 3 \times 10^7$ K and $\dot{M}_{\rm WD} = 10^{-9}\,{\rm M}_{\odot}\,{\rm yr}^{-1}$. $M_{\rm V}$ (solid blue) $M_{\rm NUV}$ (green dash) and $M_{\rm XRT}$ (black dash–dot).

4.6 Multiple outbursts

Some of the models exhibit multiple outbursts during the mass-loss phase. Prialnik & Livio (1995) first reported mass loss in two stages. Following the first mass-loss episode an envelope contraction occurred. Enhanced pressure at the envelope base then caused an increase in the nuclear luminosity, leading to re-expansion and a second mass-loss episode. Two models displaying large, multiple outbursts, are 065.10.10 and 065.30.10 (Fig. 4, panel 1). (Some of the more massive WDs exhibited multiple flashes as well.) The former continues rising in bursts throughout the entire nova until the mass loss ceases. The latter peaks and then declines back. It displays two major additional bursts of ∼2 mag in all three bands. This model (a close up of which is shown in the left panel of Fig. 9) resembles Strope et al.'s (2010) J-class (*jitters*) nova light curve (see their fig. 19 of nova V723 Cas). An example of a very different presentation of multiple outbursts of ∼1 mag is demonstrated by model 125.10.10 (Fig. 4, panel 5). A close-up is shown in the right panel of Fig. 9. In this model the first ∼5 days after outburst resemble Hounsell et al.'s (2010) SMEI light curve of V1280 Sco (see their fig. 2).

4.7 Decline – secondary rise

When the mass-loss phase is completed all models undergo a sharp luminosity drop in all three passbands. The X-ray luminosity, which was the lowest during the mass-loss phase, becomes the highest and the VIS becomes the lowest. The X-ray becomes hard at this point especially for the massive WDs as demonstrated by the effective temperature in Fig. 3 and via observations by Schwarz et al. (2011, Fig. 4). For most low-mass models, the NUV luminosity is just slightly lower than the X-ray luminosity, with the VIS falling far below. For the more massive WDs, the NUV and the VIS luminosities are both much weaker than the X-ray luminosity. Differences between the X-ray and the VIS luminosities of 2–8 mag are predicted by the models. Later, the X-ray luminosity declines as well, approaching the VIS luminosity before the beginning of the next

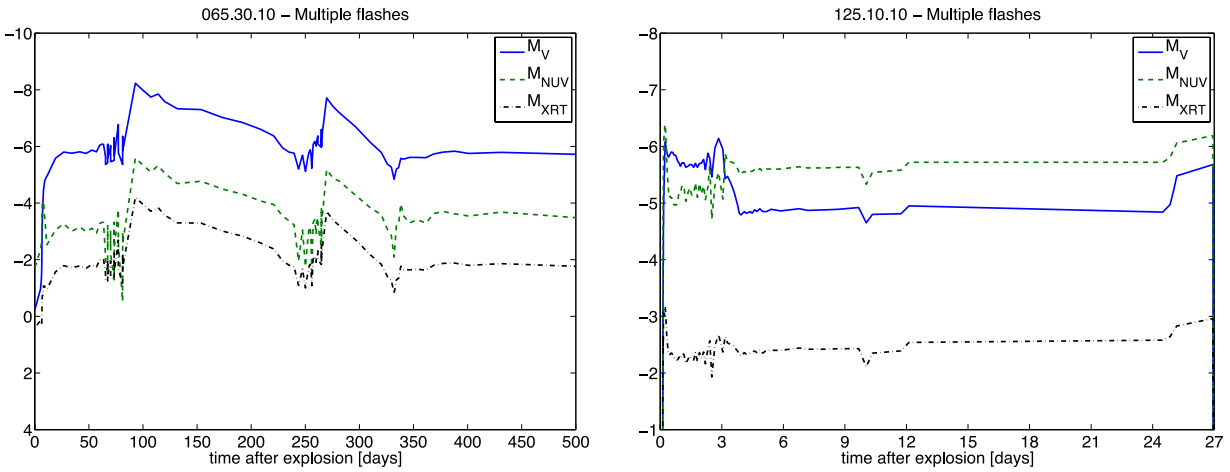

Figure 9. Left: $M_{\rm WD} = 0.65\,{\rm M}_{\odot}$, $T_{\rm c} = 3 \times 10^7$ K and $\dot{M}_{\rm WD} = 10^{-1}\,{\rm M}_{\odot}\,{\rm yr}^{-1}$ exhibiting large multiple flashes on a time-scale and amplitude similar to Strope et al.'s (2010) J-class nova light curves. Right: $M_{\rm WD} = 1.25\,{\rm M}_{\odot}$, $T_{\rm c} = 10^7$ K and $\dot{M}_{\rm WD} = 10^{-10}\,{\rm M}_{\odot}\,{\rm yr}^{-1}$ exhibiting moderate-amplitude multiple flashes on a short time-scale.

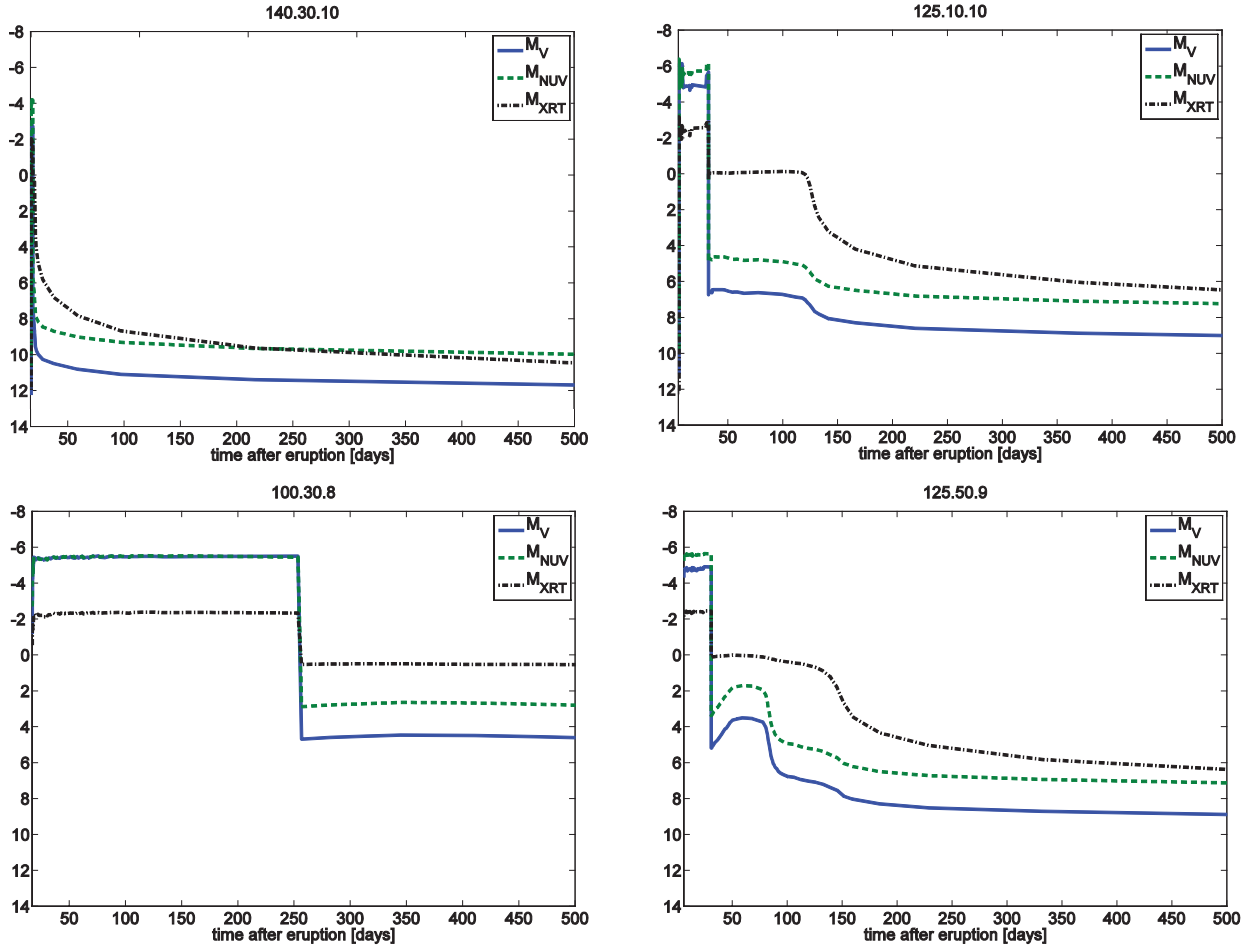

Figure 10. Decline over the first 500 d post-eruption of $M_{\rm V}$ (blue solid), $M_{\rm NUV}$ (green dash) and $M_{\rm XRT}$ (black dash-dot). Top left: $M_{\rm WD} = 1.4\,{\rm M}_{\odot}$, $T_{\rm c} = 3 \times 10^7$ K and $\dot{M}_{\rm WD} = 10^{-10}\,{\rm M}_{\odot}\,{\rm yr}^{-1}$, resembling S-class. Top right: $M_{\rm WD} = 1.25\,{\rm M}_{\odot}$, $T_{\rm c} = 10^7$ K and $\dot{M}_{\rm WD} = 10^{-10}\,{\rm M}_{\odot}\,{\rm yr}^{-1}$, resembling P-class. Bottom left: $M_{\rm WD} = 1.0\,{\rm M}_{\odot}$, $T_{\rm c} = 3 \times 10^7$ K and $\dot{M}_{\rm WD} = 10^{-8}\,{\rm M}_{\odot}\,{\rm yr}^{-1}$, resembling F-class. Bottom right: $M_{\rm WD} = 1.25\,{\rm M}_{\odot}$, $T_{\rm c} = 5 \times 10^7$ K and $\dot{M}_{\rm WD} = 10^{-9}\,{\rm M}_{\odot}\,{\rm yr}^{-1}$, a secondary rise, resembling C-class.

cycle. Pietsch (2010) reported many cases of X-ray detections long after optical decline.

Some models exhibit a secondary rise in the VIS and NUV bands (but not in the X-ray band) after the first sharp drop, as the long post-nova decline begins. These secondary rises present themselves in three slightly different ways. (1) The 100.10.11 (Fig. 4, panel 3) model has a sharp rise of ∼1 mag and slow decline, beginning ∼500 d post-nova and returning to its pre-rise values after ∼500 d. (2) The 100.50.12 (Fig. 4, panel 4) and 125.50.9 (Fig. 4, panel 6) models rise smoothly (rather than having a sharp rise) and decline smoothly as well. The total magnitude rise is of ∼1.5 mag and ∼2 mag accordingly, the rise starts immediately after the drop and the levels return to their pre-rise state after ∼150 and ∼50 d accordingly. (3) The 140.10.10 (Fig. 4, panel 6), 140.30.9, 140.50.8 and 140.50.10 (Fig. 4, panel 7) models demonstrate a very gradual rise of ∼1 mag, and a smooth decline. The rise starts immediately after the drop and the levels return to their pre-rise state after ∼1.5–2.5 d. This secondary rise corresponds to a slight increase in maximum temperature, followed by a secondary expansion causing a decrease in the effective temperature, entailing a rise in the corresponding, relatively long wavelengths – the VIS and the NUV – but not in the short-waved X-ray.

This secondary rise has been observed, and classified by Strope et al. (2010) as the C-class (*cusp*) nova light curves. Even though some aspects of the decline of nova light curves are affected by expanding dust shells, while our models describe solely the WD, there are some remarkable similarities. Fig. 10 presents examples of four types of declines, taken from our light curve data base, that resemble Strope et al.'s classification system (see their fig. 2). Their S-class (*smooth*) resembles many of our high-mass models (Fig. 10, top left), their P-class (*plateau*) resembles many of our moderate-to-high mass models (top right), their F-class (*flat top*) resembles some of our moderate mass models (bottom left) and their C-class (*Cusp*) resembles the models that demonstrate the secondary rise described above (bottom right).

5 DISCUSSION AND CONCLUSIONS

The extensive nova light curve analysis presented in this paper explains many of the detailed features seen in real novae during their eruptions, and predicts behaviours never (or rarely) seen before. In particular; (1) a pre-nova NUV flash, of amplitude ∼0.5–3 mag, will be seen lasting for a day to a week. This flash occurs in the NUV band for low-mass WDs while moderate-mass models have an accompanying X-ray flash as well. (2) A few models undergo a brief, modest-amplitude oscillation before or during the mass-loss phase. (3) The majority of our light curves displayed a pre-maximum halt of a few mag in the form of a step in the magnitude

profile, in all three passbands. The pre-maximum halt is largest in the visual and smallest in the X-ray. In many cases a dip in the total luminosity accompanied these halts immediately before the mass loss began, caused by the convection zone boundary receding from the photosphere. Most models showed these halts in all three bands. The low-mass models showed these halts in two bands (VIS and X-ray) while the massive, slowly accreting models exhibited a halt only in the X-ray band. We explored the possibility that the abundances of the heavy elements in the ejecta may be correlated somehow with the features we presented here, but found no substantial correlation. Variations in the abundance are mostly related to the WD mass and accretion rate as detailed in Yaron et al. (2005, table 2).

Some of the predicted features do resemble observations; the NUV precursor flash which resembles observations reported by Cao et al. (2012); the pre-maximum small halt, which matches visual observations of RS-Ophiuchi and KT-Eridani Hounsell et al. (2010); the oscillations and the post-nova decline behaviour, including the secondary rise, that fit well with the morphological classes O, S, P, F and C defined by Strope et al. (2010) and their J-class that resembles some of our multiple-outbursting models which might be observable (decades after outburst) as multiple shells resulting from a single nova eruption Duerbeck (1987).

Finally we note two important caveats. The light curves analysed in this work result from the luminosity of the WD only; once mass has left the photosphere of the WD, it is considered lost, and the interaction of the WD luminosity with the nebula is not calculated. Some novae form dusty nebulae, which obscure the WD and reradiate in the infrared (IR). For this reason, we have not modelled the IR passband, since most of the radiation may originate from the expanding dusty nebula. Our results refer to an unobscured WD throughout the entire cycle.

The second caveat is driven by the parameter study nature of this paper. The frequency of a phenomenon in our results (whether it be NUV flashes, oscillations, pre-maximum halts, etc.) has no implication for the likelihood of it being observed. A rare result may be from a model parameter combination that is very common in nature and vice versa.

ACKNOWLEDGEMENTS

This work was supported by Grant No.2010220 of the United States – Israel Binational Science Foundation. MS gratefully acknowledges ongoing support from Hilary and Ethel Lipsitz, and very helpful conversations with J. Mikolajewska concerning symbiotic novae. A very helpful referee report by Mike Bode is also gratefully acknowledged.

REFERENCES

Bessel M. S., 1990, A&AS, 83, 357
Bode M. F. et al., 2006, ApJ, 652, 629
Cao Y. et al., 2012, ApJ, 752, 133
Duerbeck H. W., 1987, ESO Messenger, 50, 8
Gehrels N. et al., 2004, ApJ, 611, 1005
Hounsell R. et al., 2010, ApJ, 724, 480
Itoh H., Hachisu I., 1990, ApJ, 358, 551
Kraft R. P., 1964, ApJ, 139, 457
MacDonald J., Vennes S., 1991, ApJ, 373, L51
MacDonald J., Fujimoto M. Y., Truran J. W., 1985, ApJ, 294, 263
Martin C. et al., 2005, in Colless M., Staveley-Smith L., Stathakis R. A., eds, ASP Conf. Ser. Vol. 216. IAU Symp., Maps of the Cosmos. Astron. Soc. Pac., San Francisco, p. 221
Oke J. B., 1974, ApJS, 236, 21
Orio M., Della Valle M., Massone G., Ögelman H., 1994, A&A, 289, L11
Orio M., Mukai K., Bianchini A., De Martino D., Howell S., 2009, ApJ, 690, 1753
Payne-Gaposchkin C., 1957, The Galactic Novae. Interscience, New York
Pietsch W., 2010, Astron. Nachr. 331, 187–192
Pietsch W., Sala G., Haberl F., Greiner J., 2007a, Astron. Telegram, 1149
Pietsch W., Sala G., Haberl F., Greiner J., 2007b, Astron. Telegram, 1157
Prialnik D., 1986, ApJ, 310, 222
Prialnik D., 1995, in Bianchini A., Della Valle M., Orio M., eds, Cataclysmic Variables. Kluwer, The Netherlands, p. 217
Prialnik D., Kovetz A., 1995, ApJ, 445, 789
Prialnik D., Livio M., 1995, PASP, 107, 1201
Prialnik D., Shara M. M., Shaviv G., 1978, A&A, 62, 339
Ribas I., Jordi C., Vilardell F., Fitzpatrick E. L., Hilditch R. W., Guinan E. F., 2005, ApJ, 635, L37
Schaefer B. B., Collazzi A. C., 2010, AJ, 139, 1831
Schwarz G. J. et al., 2011, ApJS, 197, 31
Shara M. M., 1989, PASP, 101, 5
Shara M. M., Prialnik D., Kovetz A., 1993, ApJ, 406, 220
Shore S. N., Kenyon S. J., Sonneborn G., 1996, ApJ, 456, 717
Starrfield S., Truran J. W., Sparks W. M., Kutter G. S., 1972, ApJ, 176, 169
Starrfield S., Iliadis C., Hix W. R., 2008, in Bode M. F., Evans A., eds, Classical Novae. p. 77
Strope R. J., Schaefer B. E., Henden A. A., 2010, ApJ, 140, 34
Yaron O., Prialnik D., Shara M. M., Kovetz A., 2005, ApJ, 623, 398

This paper has been typeset from a TEX/LATEX file prepared by the author.